

1 A sequence stratigraphic framework for the Upper Devonian Woodford Shale,
2 Permian Basin, west Texas

3

4 Nikki T. Hemmesch¹, Nicholas B. Harris^{*2,1}, Cheryl A. Mnich^{1,3}, and David Selby⁴

5

6 ¹ Department of Geology and Geological Engineering, Colorado School of Mines,
7 Golden, CO

8 ² Department of Earth and Atmospheric Sciences, University of Alberta,
9 Edmonton, Canada

10 ³ Now at: ConocoPhillips Inc., Houston, TX

11 ⁴ Department of Earth Sciences, Durham University, Durham, U.K.

12

13 * corresponding author: nharris@ualberta.ca

14

15 1 **ABSTRACT**

16

17 Criteria for recognizing stratigraphic sequences are well established on
18 continental margins but much more challenging in basinal settings. Current
19 paradigms rely primarily on assignment of high gamma ray intervals to
20 transgressive systems tracts or maximum flooding surfaces and the somewhat
21 controversial delineation of exposure surfaces in cores. This study of the Upper
22 Devonian Woodford Shale, Permian Basin, west Texas, attempts to identify sea
23 level signatures in an organic-shale through detailed sedimentological analysis of
24 long cores.

25

26 The Woodford is a prominent source of hydrocarbons and a target for shale gas
27 reserves in the Permian basin. The formation is dominated by organic-rich
28 mudstone, with interbeds of non-mudstone lithofacies including carbonate beds,
29 chert beds and radiolarian laminae, all probably deposited as sediment gravity
30 flows. Overlying the organic-rich mudstone in one well is a thick bioturbated
31 organic-poor mudstone that indicates overall shallowing-up, consistent with a 2nd
32 order global eustatic sea level fall from 386 to 359 Ma. Carbonate beds occur in
33 bundles that define a cyclicity typically 5 to 10 meters thick; these are interpreted
34 as reflecting high stand shedding. Thus intervals of interbedded carbonate and
35 organic-rich mudstone define 3rd order high stands, while the intervening
36 intervals of uninterrupted organic-rich mudstone mark low stand and
37 transgressive systems tracts. Chert beds are concentrated in the upper part of

38 the Woodford section, whereas carbonate beds are concentrated in the lower
39 part. These distributions are associated with the 2nd order sea level fall, with the
40 carbonate beds the result of high stand shedding at this time scale, while the
41 chert beds reflect increasing dissolved flux into a progressively more restricted
42 basin.

43

44 Additional effects are introduced by geographic position within the basin. Well
45 locations nearest the western margin had the greatest concentration of carbonate
46 beds due to proximity to a carbonate platform. A well near the southern margin
47 had the greatest concentration of chert, presumably the result of shedding of
48 biogenic silica from a southern platform. A well in the basin center experienced
49 minimal deposition of chert and carbonate; here, 3rd order sea level cycles were
50 primarily reflected in the distribution of radiolarian-rich laminae.

51

52 **2 INTRODUCTION**

53

54 The characterization of stratigraphic units and surfaces in the context of sea level
55 cycles, termed 'sequence stratigraphy', is now accepted as an important
56 approach to defining correlations in depositional settings from marginal marine to
57 the continental slope and adjacent abyssal plain. Sea level cycles function as a
58 clock, creating recognizable and more or less regular time markers in the
59 stratigraphic record. These markers, primarily maximum flooding surfaces and
60 unconformities, define the maximum and minimum sea level stands. The

61 sequence stratigraphy approach has also been applied to lacustrine systems,
62 where fluctuating lake levels generate correlatable units and surfaces. Here, too,
63 water level is the clock, although the beat in lacustrine systems can be orders of
64 magnitude faster than in marine systems.

65

66 The sequence stratigraphic approach is more problematic in fluvial and basinal
67 settings. In fluvial settings, it is not clear that a clock exists, at least one that
68 keeps uniform time across the entire basin. River avulsions generally do not
69 produce a basinwide signal, and subsidence events are not necessarily
70 synchronous across a basin, although a recent study by Fanti and Catuneanu
71 (2010) suggests that at least for some distance inland from the shoreline, thick
72 coal successions correlate with marine maximum flooding surfaces. Recent
73 investigations have focused on deciphering climate signals in the stratigraphic
74 records of fluvial settings, but while such signals may exist, it is not clear that
75 they are recorded in the spatial distribution of sedimentary facies or that
76 stratigraphy provide a sufficiently distinct record.

77

78 In basinal settings of large marine basins, the problem is that the signal is weak.
79 On a marine shelf, a 25 meter fall in sea level might represent a 25% change in
80 water depth and an even greater shift in proximity to a shoreline. However in the
81 middle of a basin, that same 25 meter fall in sea level might represent a 5%
82 change in water depth and a smaller relative shift in distance to a shoreline. So it
83 may be expected that the sea level signal be subtle.

84

85 In recent years, a number of workers have begun to test whether sequence
86 stratigraphic approaches can apply to basinal shales. Notable among these
87 studies are papers by Schieber (2003) and Schieber and Riciputi (2004) who
88 argued that apparently continuous sequences of black shale in the Appalachian
89 Basin in fact contain exposure surfaces, indicated by subtle erosion surfaces and
90 distinct rounded pyrite grains that are interpreted as pyritized ferrous iron-rich
91 ooids. The ooids formed during sea levels lowstands when a shale bed was
92 exposed to shallow water, oxygenated conditions and were pyritized during the
93 subsequent transgression. Such interpretations require that even at sea level
94 highstands, the maximum water depth must have been relatively shallow such
95 that the sediment-water interface was exposed to erosion during the subsequent
96 low stands.

97

98 Our study of the Upper Devonian Woodford Shale of the Permian Basin, west
99 Texas, was undertaken with the objective of defining criteria for recognizing
100 stratigraphic sequences in black shales by identifying patterns in depositional
101 facies that can be interpreted in the context of sea level changes. We report
102 here on a study of four long cores that display a variety of rock types and
103 sedimentary features, not just the classic laminated dark organic-rich mudstone
104 that is sometimes assumed to be the sole constituent of black shale. The model
105 we develop relies primarily on the stratigraphic and geographic distribution of

106 these non-shale lithofacies, which, we argue, are key to interpreting second and
107 third order sea level cycles.

108

109 **3 GEOLOGIC SETTING**

110

111 **3.1 Tectonic and Paleogeographic Setting**

112

113 The Permian Basin of west Texas, or the Tobosa Basin as Comer (1991) termed
114 its Late Devonian incarnation, formed a reentrant on the southwestern margin of
115 the North American continent (Fig. 1). It was one of several coeval basins in
116 North America in which organic-carbon-rich sediments were deposited, including
117 the Oklahoma, Black Warrior, Appalachian Basin, Illinois, Michigan, Williston and
118 Western Canada Sedimentary basins.

119

120 In the Late Devonian, the North American continent largely lay in the southern
121 hemisphere. It was also rotated clockwise relative to its present-day position,
122 such that the Permian Basin lay in a near-tropical setting at a paleo-latitude of
123 approximately 20°S. All of the North American Late Devonian basins lay within a
124 belt extending from 10° to 25°S. The global ocean lay to the south, although
125 reconstructions by Blakey (Fig. 1) suggest that much of the western part of North
126 America was flooded.

127

128 The Late Devonian Permian Basin was bounded to the north by exposed
129 continental terrane of the Trans-Continental Arch, locally called the Pedernal
130 Uplift or Massif (Fig. 2); schists and granites have been dated at 1471 and 1364
131 Ma (Mukhopadhyay et al., 1975). The eastern and western margins of the basin
132 are less constrained. The eastern margin was formed by the Concho Arch; this
133 was thought by Comer (1991) to be emergent, by Algeo et al. (2007) to be
134 submerged, and by others (Perkins et al. 2008) to be non-existent. The western
135 margin is more obscure. An Ordovician positive feature along present-day Rio
136 Grande River, termed the Diablo Platform, was the site of shallow water
137 carbonate deposition (Goldhammer et al. 1993). Comer (1991) suggested that
138 this feature persisted through the Late Devonian. However no direct evidence of
139 Upper Devonian in-place shallow water carbonate sediments exists, and
140 consequently its existence must be inferred from facies relationships within the
141 basin.

142

143 The Central Basin Platform, which during the Permian separated the Delaware
144 Basin from the Midland Basin, did not exist in the Late Devonian; however,
145 Ellison (1950) and Comer (1991) noted that the Upper Woodford is anomalously
146 thin along the Central Basin Platform and the Northwest Shelf. Comer (1991)
147 suggested that vertical movements along ancestral structures were related to
148 tectonism at a distance along other continental margins: the Acadian Orogeny in
149 northeastern North America and the Antler Orogeny in western North America.
150 The eastern part of the Permian Basin was interpreted by Comer (1991) as

151 having been relatively shallow in the Late Devonian, as were the Northwestern
152 and Eastern Shelves. He noted that the thickest, most complete Woodford
153 sections were found in the areas of the Delaware and Val Verde Basins,
154 suggesting that these areas were the deepest parts of the Late Devonian
155 Permian Basin.

156

157 **3.2 Silurian through Mississippian Stratigraphy**

158

159 The Woodford Shale is part of a Paleozoic succession dominated by carbonate
160 and shale successions (Figure 3). It overlies the Lower to Middle Devonian
161 Thirtyone Formation in the Delaware Basin and coeval Devonian Limestone in
162 the Midland Basin and on the Central Basin Platform, separated by a regional
163 unconformity that elsewhere in the Midcontinent removed older Devonian and
164 some Silurian strata. Comer (1991) reported that 'cavernous limestone'
165 underlies black shale in a well from Lea County, New Mexico, suggesting that
166 this unconformity was at least locally accompanied by prolonged exposure and
167 karst development.

168

169 The Woodford is unconformably overlain by the Rancheria Formation in the
170 Delaware Basin and the Mississippian Limestone in the Midland Basin and on
171 the Central Basin Platform. In the Delaware Basin, the time interval represented
172 by the unconformity includes the Kinderhookian, Osagean and part of the
173 Meramecian stages, a period of approximately 20 million years.

174

175 Comer (1991) reports dates of latest Givetian to earliest Mississippian for the
176 Woodford. A subsequent conodont study, sampling wells in the Midland Basin
177 (eastern Permian Basin) (Meyer and Barrick, 2000) restricted the age of organic-
178 rich shale somewhat; they described a 'pre-Woodford' green and grey shale with
179 latest Givetian and Frasnian conodonts and a typical Woodford, organic-rich
180 black shale with middle to late Famennian conodonts.

181

182 **3.3 Woodford Stratigraphy and Regional Correlations**

183

184 Ellison (1950) and subsequently Comer (1991) recognized that the Woodford can
185 be divided into three members, based on gamma log response. These members
186 are correlative regionally across the basin; our work here is consistent with this
187 previously developed stratigraphy. The members include a Lower Woodford
188 member with relatively low gamma ray, a Middle Woodford member with
189 remarkably high gamma ray, and an Upper Woodford member with relatively low
190 gamma ray. Even the lower gamma ray signatures of the Lower and Upper
191 members are high in the context of most shales; both units commonly has
192 gamma ray readings of 100 to 200 API units, but gamma ray readings in the
193 Middle Woodford are typically 300 to 500.

194

195 The Woodford in the Permian Basin is correlative with the upper part of the
196 Caballos Novaculite in the Marathon region of west Texas, the Percha Formation

197 in Hueco and Franklin Mountains of west Texas, and the Sly Gap Formation of
198 southeastern New Mexico. The Percha is a black, fissile, non-fossiliferous shale,
199 whereas the Sly Gap Formation is a fossiliferous tan to pale yellow shale,
200 siltstone and limestone (Comer 1991).

201

202 3.4 Dataset and Methods

203

204 Our data come from long cores in four wells in west Texas: the Reliance Triple
205 Crown (RTC) #1 well (290 feet; 88.4 m) and the La Escalera B55 well (174 feet;
206 53.0 m) in western Pecos County, the Keystone Cattle Company (KCC) 503 well
207 in Winkler County (303.5 feet; 92.5 m), and the MBF well (250 feet; 76 m) in
208 Reeves County. These cores represent 78%, 61% and 52% of the total
209 Woodford thickness at the locations of the first three wells; we were not provided
210 logs for the MBF well and do not know the thickness of the complete Woodford
211 section at this location.

212

213 The cores were initially described in detail at a scale of 1:16; condensed versions
214 of the descriptions shown in Figures 4 to 7. Original descriptions included:
215 identification of lithologies, sedimentary structures including both physical
216 lamination and bioturbation, the presence of cements including calcite, dolomite
217 and pyrite, and the presence, intensity and orientation of fractures relative to
218 vertical. The RTC #1 and KCC 503 cores were sampled for petrographic thin
219 sections; these were found invaluable for corroborating lithologic identification,

220 documenting bedding styles in very fine-grained rocks, and identifying
221 microfossils. Additional samples were taken for geochemical analysis (Mnich
222 2009).

223

224 Cores were correlated to electric logs provided to us by the well operators:
225 Pioneer Natural Resources (RTC #1 well); Petro-Hunt (B55 well); and Whiting
226 Petroleum (KCC 503 well). These logs included both wireline and core gamma
227 logs, which were invaluable in correlating cores to logs.

228

229 Radiometric age dates were obtained on four samples from the RTC#1 core
230 using the Re-Os method. Samples were selected to obtain a wide stratigraphic
231 range and picked to avoid any evidence of hydrothermal alteration (filled
232 fractures or veins).

233

234 4.0 RESULTS

235

236 4.1 Lithofacies

237

238 Five lithofacies are present throughout most of the Woodford: mudstone,
239 mudstone with phosphate nodules, dolomite, bedded chert, radiolarian-carbonate
240 laminae, bioturbated mudstone and massive chert (novaculite).

241

242 4.1.1 Mudstone

243

244 Mudstone is the overwhelmingly dominant lithology in the Woodford, amounting
245 from 85 to 99% of the formation in all wells (Figures 4 to 7). This rock is
246 composed predominantly of quartz and clays in proportions from 1.5:1 to 8:1,
247 with quartz content increasing upward through much of the formation (Mnich,
248 2009; Harris et al., 2009). Total organic carbon (TOC) content ranges from 1 to
249 14 weight % and, based on the gamma ray log that is highly correlative with
250 TOC, appears to be cyclically distributed. Dolomite is a significant component of
251 mudstone only near the base of the formation. Minor components of the shale
252 include pyrite and feldspar. The mudstone is not notably fossiliferous.

253 Tasmanites cysts are dispersed throughout (Fig. 10E), as are recrystallized
254 radiolarian. We have tentatively identified agglutinated foraminifera.

255

256 The mudstone is variably laminated, in places displaying a distinct submillimeter-
257 scale parallel lamination (Figs. 8A, 10A), but elsewhere faintly bedded or
258 massive (Fig. 8B). Discerning lamination is surprisingly difficult, even when
259 digital photos have been processed to enhance features and even in thin section.
260 Considerable effort was devoted to resolving whether the massive nature was
261 real, and if so, whether it was a primary physical depositional fabric or resulted
262 from bioturbation.

263

264 Laminae in the finely laminated mudstones displays subtle pinching and swelling
265 at a scale of 2-4 cm, although truncations of laminae were not noted. Laminae

266 also display disruptions, suggesting a bioturbated fabric, although definitive
267 burrow structures were not identified. Massive mudstones lack vertical changes
268 in grain size or composition, but nonetheless have a planar fabric defined by the
269 orientation of organic particles such as flattened Tasmanites cysts, foraminifera or
270 clay.

271

272 Disturbed or convolute bedding, interpreted as soft sediment deformation, is
273 relatively rare. One 10 foot thick (3 meter) section from the La Escalera core
274 contains discordant bedding and locally flow folds; we have interpreted this as a
275 large slumped interval..

276

277 Two additional sedimentary features are common. One is a flared structure of
278 white carbonate (Fig. 8C), associated with a thin brittle layer, typically 2 to 3 cm
279 in height and 4 cm in diameters. We assume that they are conical in form but
280 were not able to see them in plan view. We interpret these as fluid escape
281 structures, either gas or water. A second structure consists of thin highly
282 convoluted sheets (Fig. 8D), commonly 2 cm in height; in plan view, they are
283 linear and at least a few cm long. These are interpreted as syneresis cracks,
284 nearly syndepositional features that were originally planar but became
285 convoluted during compaction. It is common to see multiple such features
286 restricted to a single bed that presumably a fair degree of cohesiveness just after
287 deposition.

288

289 4.1.2 Dolomite

290

291 Dolomite is found in discrete beds from 1 to 30 cm thick, commonly in the range
292 of 2 to 8 cm (Figs. 9A, 10B). Dolomite is micritic to silt-size in these beds, locally
293 exhibiting subtle grading in the uppermost one to two millimeters. Recognizable
294 bioclasts are virtually never present; one bryozoan fragment was found. The
295 thickest of the beds, in the lower part of the section in the RTC #1 well, contained
296 several dark mudstone clasts, identical to the mudstones. One bed is composed
297 of what appear to be fragments of laminated dolomite; we interpret these a
298 broken and redeposited fragments of a dolomite crust. Beds are largely massive
299 but rarely show parallel lamination in the thickest beds.

300

301

302 4.1.3 Bedded Chert

303

304 Chert occurs in beds generally 3 to 10 cm thick (Fig. 9C). The chert is extremely
305 hard, dark (in fact similar in color to and sometimes difficult to distinguish from
306 the mudstone) and contains internal vertical fractures. It is composed of
307 radiolaria that are variously recrystallized and small amounts of clay and
308 carbonates. The chert is massive to laminated on a scale less than 1 mm and
309 may show grading from 100% upward into fine grain material, typically fine
310 quartz, clay and organic matter.

311

312 4.1.4 Radiolarian laminae

313

314 Radiolaria are concentrated in laminae 2 mm or less in thickness (fig. 8F and
315 10C) that also contain fine grained material, including quartz, organic matter and
316 clay. Coarse carbonate, probably dolomite is commonly present in these
317 laminae, which we interpret as a diagenetic product. These laminae are sharp-
318 based and may have sharp or gradational tops.

319

320 4.1.5 Mudstone with phosphatic nodules

321

322 The mudstone locally contains numerous phosphatic concretions (Fig. 8E) in two
323 narrowly defined stratigraphic intervals, one in the Upper Woodford in the RTC
324 #1 and MBF cores a few meters above the gamma log break defining the Middle
325 Woodford – Upper Woodford boundary (Figs. 4 and 6), comprising approximately
326 10% of the section. One additional interval of phosphatic concretions was noted,
327 a 1.5 meter thick section in the Lower Woodford section of the La Escalera core.
328 These concretions are irregularly flattened parallel to bedding, generally 3 to 5
329 cm in thickness and 5 to 10 cm in length. They consist of apatite and quartz
330 (chert), in which apatite crystals form euhedral crystals in a groundmass of
331 microcrystalline quartz (Fig. 10D).

332

333 4.1.6 Massive chert (novaculite)

334

335 Two types of chert are present near the top of the section: a white and a dark
336 grey chert (Figs. 6 and 9D). These are enriched in quartz relative to the
337 underlying and overlying mudstones, as reported by Chesapeake from XRD
338 analysis (78% in one sample), with minor illite/smectite (17%), feldspar (5%) and
339 pyrite (1%). We lack the data to account for color differences between the two
340 types of chert.

341

342 This unit may be a tongue of the Caballos Novaculite, the top of which is dated in
343 the Marathon Basin at upper Frasnian or lowermost Kinderhookian (Noble,
344 1992).

345

346 4.1.7 Bioturbated mudstone

347

348 The dark, organic carbon-rich mudstone is sharply overlain by a lighter grey,
349 pervasively bioturbated mudstone in the MBF well (Figs. 6 and 9E). Sedimentary
350 structures are rarely visible in this interval (bioturbation index of grade 5 or 6,
351 following the classification of Taylor and Goldring, 1993); the rare preserved
352 structures are thin wavy laminae. The burrowing appears to be dominated by
353 simple small burrows, although textures were indistinct. Possible rare large
354 Teichicnus burrows were found, suggesting fully oxygenated conditions in mid- to
355 outer shelf water depths.

356

357 Mineralogical composition of the bioturbated mudstone is similar to the
358 underlying organic-rich mudstone. Quantitative XRD reports from Chesapeake
359 indicate compositions dominated by quartz (average of 4 samples was 61%) and
360 illite/smectite (23%) with subordinate feldspar (8%) and dolomite (3%). Total
361 organic carbon contents in this facies are greatly reduced in comparison with the
362 underlying dark mudstone. TOC data provided by Chesapeake averaged 0.86%
363 in this interval (Fig. 6).

364

365 4.2 **Geographic distribution of lithofacies**

366

367 The distribution of lithofacies varies substantially between the four wells studies
368 here. Two key points include:

369

370 (1) Carbonate beds are most common in the western wells, the MBF (60
371 individual beds) and RTC #1 wells (38 beds). Moreover, the upper part of
372 the Upper Woodford was truncated by erosion in the RTC #1 well, so the
373 pre-erosion section might have contained more carbonate. Only 17 beds
374 were identified in the La Escalera core and 6 were identified in the long
375 KCC #1 core (although this core is similar in length to the RTC#1 core, it
376 covers a shorter stratigraphic interval because the Woodford section
377 expends in the basin center.

378

379 (2) Chert beds are most common in the southernmost well, the Petro-Hunt La
380 Escalera well (166 beds). They are less common in the RTC #1 well (16
381 beds) and relatively rare in the two northernmost wells, the KCC 503 and
382 MBF (5 beds in each).

383

384 Bioturbated mudstone and novaculite are present only in the Chesapeake MBF
385 core may not be significant. However, the upper part of the Upper Woodford
386 section was truncated by erosion in the RTC #1 well, removing the equivalent
387 section, and this part was not cored in the KCC 503 and La Escalera wells.

388

389 **4.3 Vertical distribution of facies**

390

391 The distribution of facies is shown in Figures 3 through 6. Most of the formation
392 is organic mudstone with interspersed chert and dolomite beds and radiolarian
393 laminae. This organic-rich section is overlain by, in succession, mudstone with
394 phosphate nodules, an additional interval of organic-rich mudstone, chert
395 (novaculite) and bioturbated organic-poor mudstone.

396

397 Within the overall succession are some distinctive patterns to the distribution of
398 carbonate and chert beds within the organic-rich mudstone. Chert beds are
399 generally concentrated in the upper part of the formation. This is particularly the
400 case in RTC #1 core (Fig. 4), where the lowermost chert beds occur just below
401 the Middle Woodford – Upper Woodford contact and are common up to the top of

402 the core. In the KCC 503 well (Fig. 5), chert beds are clustered around the high
403 TOC / high gamma ray spike near the Middle Woodford Upper Woodford contact.
404 In the La Escalera core (Fig. 7), where chert beds are most abundant and are
405 present throughout the entire core, there is still a greater concentration in the
406 upper part of the section.

407

408 The stratigraphic distribution of carbonate beds varies between wells. In MBF
409 well, carbonate beds are most abundant in the middle of the section and
410 immediately below the transition to novaculite (Fig. 6). As noted above, we lack
411 electric logs for this well and cannot place the data exactly with respect to the
412 Lower, Middle and Upper Woodford units. In the RTC #1 well, carbonate is
413 clearly preferentially distributed in the lower part of the section (Fig. 4), a
414 distribution approximately antithetic to the chert.

415

416 A cyclic distribution of carbonate beds is evident in the RTC #1 core (Fig. 4). The
417 carbonate beds occur in bundles, intervals in which their occurrence is common,
418 separated by intervals in which no carbonate is present. At least 10 such cycles
419 are evident in the RTC #1 core, ranging in thickness from 6 meters (19 feet) to 14
420 meters (46 feet). There are no obvious patterns to the vertical distribution of
421 cycle thickness or to the relative proportions of sections with and without
422 carbonate beds. The thickest beds are found near the base of the section, but
423 the thickness of the beds does not obviously vary within cycles.

424

425 A cyclicity is also evident in the radiolarian laminae in the KCC 503 core (Fig. 5).
426 These laminae also occur in bundles, concentrated in some intervals with
427 densities of 2.5 / meter, while intervening intervals have from 0 to 1 / meter. In
428 the 93 meters of cored section in this well, 3.5 cycles are present, so each cycle
429 averages 26.5 meters. However, the overall Woodford section has expanded by
430 approximately 200%, so the relative thickness of each cycle is approximately
431 similar between the two wells.

432

433 Our data from the RTC #1 and KCC 503 wells (Figs. 4 and 5) suggest that the
434 radiolarian bundles and dolomite bundles are antithetically organized, that the
435 dolomite beds are concentrated where the radiolarian laminae are sparse and
436 vice versa. That is clearly the case in the KCC 503 well, where dolomite beds
437 are uncommon. This organization is less clearly in the RTC #1 but is
438 nonetheless a plausible interpretation.

439

440 **4.4 Age dates**

441

442 The lowermost sample, from the Lower Woodford, was dated at 379.0 ± 7.9 Ma
443 (middle Frasnian) (Fig. 4). Samples from the lower and upper parts of the Middle
444 Woodford were dated at 371.5 ± 5.8 Ma and 364.0 ± 13 Ma, respectively
445 (spanning the Famennian). The uppermost sample, from the Upper Woodford,
446 was dated at 357.9 ± 5.3 Ma (Tournaisian – lowermost Mississippian).

447

448 Sedimentation rates calculated from these dates yields a best estimate of 4.04
449 meters of sediment (compacted) deposited per million years for the RTC #1
450 section, with a range of possible sedimentation rates based on the uncertainty in
451 individual ages of 3.03 to 5.40 meters per million years. Sedimentation rates
452 appear to have been remarkably constant through time.

453

454 **5 DISCUSSION**

455

456 **5.1 Depositional Processes**

457

458 Three primary mechanisms exist for transport of mud into basinal settings:
459 pelagic fallout of suspended material, traction deposits or sediment gravity flows
460 of different types. The latter may include mass flow deposits, true turbidites and
461 the recently described wave-enhanced sediment gravity flows (Macquaker et al.,
462 2010). The latter describes beds with a lower silt or very fine-grained sand layer
463 with ripple laminae, a middle layer of silt and clay with wavy parallel lamination
464 and a draping upper layer of silt and clay. Traction deposits consist of ripple
465 cross-laminated muds; these have been produced in flume experiments
466 (Schieber and Southard, 2009) and observed in the rock record (Schieber and
467 Yawar, 2009). Identification of such ripple structures in core can be difficult
468 because the low initial amplitude of the structures and the high degree of
469 compaction in mudstones.

470

471 Woodford mudstones range from finely laminated to poorly laminated to massive.
472 Even the finely laminated mudstones exhibit 'ragged' lamination. We suggest
473 that suggest that components of mudstone were introduced to the deep basin
474 through different processes. Fine grained carbonate originated on basin margin
475 platforms and was transported to the basin as sediment gravity flows. Clays
476 were introduced from the Pedernal Massif to the north; it probably accumulated
477 initially on a shallow water shelf and was then transported and redeposited in the
478 deep basin by mud flows and turbidity currents. Other components, specifically
479 organic matter and radiolarian, formed in the water column and sank to the
480 bottom as pelagic rain, possibly as floccules (Macquaker et al., 2010). Pinching
481 and swelling of laminae suggests that sediments were reworked by bottom
482 currents. Modification by bioturbation is likely, although we it is difficult to identify
483 discrete burrow structures.

484

485 Interpretation of the non-mudstone facies is more straightforward The dolomite
486 beds have many characteristics of classic turbidite beds: they are largely
487 massive, with sharp bases and subtle grading at the top to finer sediments. A
488 few beds exhibit parallel lamination. The thickest dolomite bed contains rip-up
489 clasts of black mudstone, indicating that it was incorporated into a turbidity
490 current with sufficient energy to scour the underlying muddy substrate.

491

492 The radiolarian laminae are also probably turbidite deposits, although this
493 interpretation is less definitive than that of the dolomite beds.

494

495 The chert beds can also be interpreted as turbidites. They have sharp bases,
496 commonly show an upward decrease in radiolarian spherules and an upward
497 increase in the content of fine-grained material (clay and organic matter) and are
498 planar laminated. Radiolarian chert beds that originated as turbidites are
499 described elsewhere, for example Swarbrick (1967) and Sedlock and Isozaki
500 (1990). This model implies that radiolaria must have locally accumulated in
501 shallower water as uncemented sediment and were then transported under the
502 influence of gravity and redeposited in basinal settings. One other possible origin
503 should be considered, however. These may have originated as a pelagic rain-out
504 of radiolaria from the water column. The great abundance would have been the
505 result of a nutrient slug to the basin, and the grading upward to a normal
506 mudstone the result of depletion of the water column.

507

508 **5.2 Sea Level**

509

510 5.2.1 Second order sea level cycle

511

512 The stratigraphic progression of Woodford lithofacies is from organic-rich
513 mudstone with no bioturbation (or possibly local cryptobioturbation) upward to
514 heavily bioturbated organic-poor mudstone with an infauna characteristic of mid-
515 shelf depths. This suggests that water depths decreased significantly during
516 deposition of the Woodford. This interpretation is consistent with organic

517 petrology data from the RTC #1 well, which shows a distinct increase in the
518 fraction of terrestrial kerogen in the Upper Woodford (Mnich, 2009).

519

520 Physical sedimentary structures are consistent with this interpretation. In the
521 organic-rich mudstones, coarse sediment was introduced only through the action
522 of sediment gravity flows; there is no indication of persistent traction currents. In
523 the bioturbated mudstone at the top of the Woodford section, remnants of wavy
524 bedding are preserved that are consistent with an interpretation of fair-weather or
525 storm wave influence, in other words inner to mid shelf depths.

526

527 Decreasing water depths could have resulted either (1) a fall in eustatic sea level,
528 (2) sedimentation outpacing subsidence, or (3) tectonism. In this case, we and
529 others see little evidence for orogenic uplift, so it is unlikely that there was a
530 tectonic component to basin shallowing. Eustacy, however, could have been a
531 significant contributor to shallowing. Haq and Schutter (2008) describe a 2nd
532 order sea level fall of approximately 70 meters from the earliest Frasnian to the
533 latest Famennian. Moreover, two extreme 3rd order sea level falls occurred
534 within the Tournaisian, one at the Famennian-Tournaisian boundary and a
535 second approximately 6 m.y. later. Both were on the order of 100 meters,
536 superimposed on the 70 meter 2nd order fall. So a total sea level fall of 170
537 meters is possible, based solely on eustacy.

538

539 Within the basin, 90 to 200 meters of shale were deposited over a period of
540 approximately 20 million years. Assuming Airy isostasy, then crustal subsidence
541 due to sedimentation alone would have amounted to X meters during this time;
542 thus the basin would have shallowed by XXX meters. The combined effect of
543 eustatic sea level fall and sedimentation would have been a decrease in sea
544 level of XX meters.

545

546 If we assume, fairly arbitrarily, a water depth of 50 meters for deposition of the
547 bioturbated mudstone, that would place water depth at the start of organic
548 mudstone deposition at approximately XX.

549

550 5.1.2 Third order sea level cycles

551

552 The distinctive bundling of carbonate beds in the RTC #1 core can be interpreted
553 as a product of high stand shedding. This process is associated with
554 carbonate platforms and has been described in many Quaternary platforms and
555 is manifested in maximal transport of shallow water carbonate to the adjacent
556 deep basin during sea level high stands (Schlager et al., 1994). It depends on
557 three relationships: (1) carbonate production is greatest during highstands when
558 large areas of the platform are shallowly submerged, yet accommodation space
559 is minimal; (2) carbonate production decreases during transgressions when the
560 platform is deeply submerged, at the same time when accommodation space

561 increases; (3) carbonate production is also low during low stands when
562 carbonate platforms are exposed.

563

564 The bundles of dolomite beds therefore indicate sea level high stands. We
565 identify at least 10 of these in the RTC #1 core (Figure XX); more may be present
566 if these can be subdivided. This number is broadly consistent with 16 3rd order
567 eustatic cycles between the 2nd order sea level high stand in the earliest Frasnian
568 to the 2nd order low stand at the Devonian – Mississippian boundary (Haq and
569 Schutter, 2008). In general, sea level oscillations during the Frasnian are
570 relatively muted in amplitude, typically 30 meters; the amplitude is 50 to 60
571 meters during the Famennian.

572

573 If the intervals with abundant dolomite beds represent sea level high stand
574 systems tracts, then the intervening sections without dolomite beds represent the
575 low stand and transgressive systems tracts, and the sequence boundary
576 boundary should be placed at or just above the uppermost dolomite bed in each
577 bundle. We see no obvious change in continuous mudstone section that might
578 represent either the sequence boundary or the transition between low stand and
579 transgressive systems tracts. We surmise that the bulk of that interval is
580 represented by the transgressive systems tract.

581

582 Our data from the RTC #1 core suggest that the radiolarian laminae are
583 concentrated in intervals in which the carbonate beds are absent, although the

584 relationship is not clear cut. We offer a possible explanation for this. Radiolarian
585 may proliferate during low stands and in the early part of transgressions because
586 dissolved silica may be more concentrated in the water column than during high
587 stands (Mnich, 2009). The bulk of the dissolved silica must be derived from
588 chemical weathering of the continental terrane north of the basin. During low
589 stands, more continental terrane is exposed, so the flux of dissolved silica to the
590 basin should be greater. Moreover, the volume of water in the basin is less
591 during the low stands, with the combined effect being a substantial increase in
592 silica concentration.

593

594 The Woodford data allow us to test common models for interpreting stratigraphic
595 sequences and for organic carbon enrichment. High gamma ray values are
596 commonly used as a basis for identify transgressive systems tracts and
597 maximum flooding surfaces. This relationship could be due to (1) high clay
598 content during transgressions, as the deposition of coarse clastics shifts
599 landward, or (2) a model that organic carbon deposition increases during
600 transgressions, perhaps the result of lack of dilution by clastics. Figure 11
601 displays the gamma ray log and our TOC data in relationship to our inferred 3rd
602 order sea level cycles in the RTC #1 core. In this case, high gamma ray values
603 are associated with high uranium content, not high clay content, based on
604 spectral core gamma logs; in fact the contribution of potassium to the total
605 gamma ray log is fairly small. The data in Figure 11 shows that in the lower half
606 of the Woodford, in fact the highest gamma ray and TOC values correspond to

607 the carbonate bundles – in other words the high stand systems tracts, whereas
608 TOC values are lower in the low stand and transgressive systems tracts. That
609 relationship reverses in the upper half of the Woodford, where TOC values are
610 highest during the lowstand and/or transgressive systems tracts. That the
611 relationship changes suggests a basic change in the mechanism of organic
612 carbon accumulation.

613

614 5.2.3 Distribution of carbonate and chert beds

615

616 In the RTC #1 well, carbonates are largely restricted from that point to the bottom
617 of the formation. We suggest that the same mechanisms described above for 3rd
618 order cycles also apply to these beds at a 2nd order scale. Sea level was near a
619 2nd order high stand during the Frasnian, so that when 3rd order high stands
620 occurred, the platform was highly productive and significant volumes of
621 carbonate were shed to the adjacent basin. In the Famennian, however, as the
622 2nd order low stand was approached, even during high stands the platform may
623 have been partially exposed, thus minimizing carbonate production and
624 shedding.

625

626 Chert beds may also be governed by the same processes at 2nd and 3rd order
627 scales. Chert beds in the RTC #1 well occur from the upper part of the Middle
628 Woodford to the top of the formation but are not found below. Similar
629 relationships are present in the La Escalera core. Dissolved silica concentrations

630 would have been generally lower during the Frasnian 2nd order high stand, so
631 radiolarian productivity could have been less. During the 2nd order sea level fall
632 to the Devonian-Mississippian boundary, silica concentrations should have
633 increased. Moreover, if the chert beds are detrital in origin, with siliceous
634 sediment transported as turbidites, then the 2nd order sea level fall could have
635 forced migration of the source area toward the basin center.

636

637 In the KCC 503 core, the five chert beds are clustered around a high TOC spike
638 at the top of the Middle Woodford. This suggests that organic productivity and
639 nutrient delivery were also factors in the distribution of chert beds.

640

641 **5.3 Paleogeographic controls**

642

643 Location within the basin also clearly played a substantial role in the stratigraphic
644 record. Significant differences in lithofacies exist between the wells: (1) Chert
645 beds are abundant in the La Escalera well throughout the core, but are present
646 only in the upper part of the section in RTC #1 and are rare in the KCC 503 core.
647 This suggests a southern source for the radiolaria. (2) Carbonate beds are
648 abundant in the MBF cores and abundant in the lower and middle Woodford
649 sections in the RTC #1 core. They are rare in the other cores. These
650 relationships suggest that a carbonate platform existed to west of the Permian
651 Basin, as suggested by Comer (1991), and that only the proximal wells (MBF and

652 RTC #1) were close enough to the proposal to receive much carbonate
653 sediment.

654

655 5.4 Other criteria for recognizing stratigraphic sequences

656

657 No evidence for exposure surfaces exists in the Woodford cores. We are aware
658 that truncations in mudstone formations may display very low angles (Schieber,
659 2003) and can therefore be difficult to recognize in core but nonetheless found no
660 such features in either hand specimen or thin section examination. We also
661 found no features resembling the pyritized chamositic ooids described by
662 Schieber and Riciputi (2004), which they associate with erosional surfaces and
663 interpret to have formed originally as iron clay ooids in an oxygenated water
664 column. The absence of these features suggests that water depths during
665 deposition of the much of the Woodford section were great enough so that the
666 sediment was never subaerially exposed.

667

668 6 CONCLUSIONS

669

670 The Woodford Shale exhibit a number of sedimentological and stratigraphic
671 features that, when integrated, can be used to formulate a 2nd and 3rd order
672 sequence stratigraphic framework. Features indicative of a 2nd order sea level
673 fall are (1) a transition upward from organic-rich non-bioturbated or crypto-
674 bioturbated mudstone to organic-poor highly bioturbated mudstone, (2) a change

675 upward from amorphous, algal-derived organic matter to terrestrial organic
676 matter, (3) phosphate nodules near the top of the organic-rich mudstone, and (4)
677 increased frequency of chert beds and decreased frequency of carbonate beds in
678 the upper part of the section. In part these are depositional effects, related to the
679 changing balance between carbonate production and accommodation space
680 (beds of allochthonous carbonate). In part these are related to oxygen levels in
681 the paleowater column, which impacts the viability of a vigorous infauna (degree
682 of bioturbation) and early diagenetic reactions in the sediment (phosphate
683 precipitation). Finally, we suggest that the changing balance between chemical
684 runoff, specifically dissolved silica, and the size of the water mass in the basin
685 results in enhanced chert formation.

686

687 Third order sea level cycles are revealed by cyclicity in non-mudstone facies,
688 specifically beds of allochthonous carbonate, deposited as turbidites, and
689 radiolarian-rich laminae, which probably also represent deposition from sediment
690 gravity flows. Carbonate beds interbedded with organic-rich mudstone represent
691 the highstand systems tract; we invoke a model of high stand shedding to
692 account for the carbonate. The sequence boundary is placed at or just above a
693 transition to continuous organic mudstone, which in turn represent the low stand
694 and transgressive systems tracts. These 3rd order cycles are typically 5 to 12
695 meters thick. Taken together, the Woodford represent the falling sea level half of
696 a 2nd order cycle and at least 10 complete 3rd order cycles.

697

698 We suggest that two features classically associated with stratigraphic sequences,
699 either high gamma ray values due to concentrations of clay or organic matter
700 indicating flooding surfaces, or exposure surfaces indicating sequence
701 boundaries, are absent from the stratigraphic record in the Woodford Shale.
702 While a cyclic pattern of high gamma ray values is present, it reflects high TOC
703 and not high clay content; moreover, the high TOC in parts of the section is
704 associated with high stands and not transgressions. Nor do we see evidence for
705 exposure surfaces or systematic occurrence of shallow water deposition until the
706 top of the section.

707

708 **7 REFERENCES**

709

710 Algeo, T.J., Lyons, T.W., Blakey, R.C., and Over, D.J., 2007, Hydrographic
711 conditions of the Devonian-Carboniferous North American Seaway inferred from
712 sedimentary Mo-TOC relationships: *Palaeogeography, Palaeoclimatology,*
713 *Palaeoecology*, v. 256, p. 204-230.

714

715 Comer, J.B., 1991, Stratigraphic analysis of the Upper Devonian Woodford
716 Formation, Permian Basin, west Texas and southeastern New Mexico: Texas
717 Bureau of Economic Geology Report of Investigations No. 201, 63 pp.

718

719 Ellison, S.P., Jr., 1950, Subsurface Woodford black shale, west Texas and
720 southeast New Mexico: Bureau of Economic Geology, Report of Investigations,
721 No. 7, 20 p.

722

723 "Permian Basin." *Encyclopædia Britannica. Encyclopædia Britannica Online Academic*
724 *Edition*. Encyclopædia Britannica Inc., 2012. Web. 27 Feb. 2012.

725

726 Fanti, F. and Catuneanu, O., 2010, Fluvial sequence stratigraphy; the Wapiti
727 Formation, west-central Alberta, Canada: *Journal of Sedimentary Research*, v.
728 80, p. 320-338.

729

730 Goldhammer, R.K., Lehmann, P.J., and Dunn, P.A., 1993, The origin of high-
731 frequency platform carbonate cycles and third-order sequences (Lower
732 Ordovician El Paso Gp, west Texas): Constraints from outcrop data and
733 stratigraphic modeling: *Journal of Sedimentary Petrology*, v. 63, p. 318-359.

734

735 Haq, B.U., and Schutter, S.R., 2008, A chronology of Paleozoic sea-level
736 changes: *Sciences*, v. 322, no. 5898, p. 64-68.

737

738 Harris, N.B., Hemmesch, N.T., Mnich, C.A., Aoudia, K., and Miskimins, J., 2009,
739 An integrated geological and petrophysical study of a shale gas play: Woodford
740 Shale, Permian Basin, west Texas: *Gulf Coast Associations of Geological*
741 *Societies, Transactions*, v. 59, p. 337-346.

742

743 Macquaker, J.H.S., Bentley, S.J., and Bohacs, K.M., 2010, Wave-enhanced
744 sediment-gravity flows and mud dispersal across continental shelves:
745 Reappraising sediment transport processes operating in ancient mudstone
746 successions: *Geology*, v. 38, p. 947-950.

747

748 Macquaker, J.H.S., Keller, M.A., and Davies, S.J., 2010, Algal blooms and
749 “marine snow”: mechanisms that enhance preservation of organic carbon in
750 ancient fine-grained sediments: *Journal of Sedimentary Research*, v. 80, p. 934-
751 942.

752

753 Meyer, B.D., and Barrick, J.E., 2000, Conodonts from the Woodford Formation
754 (Late Devonian) and adjacent units, subsurface west Texas and eastern New
755 Mexico, *in* DeMis, W. D., Nelis, M. K., and Trentham, R. C. (eds.), *The Permian*
756 *Basin: Proving ground for tomorrow’s technologies: West Texas Geological*
757 *Society, Publication 00-109, p. 229-237.*

758

759 Mnich, C.A., 2009, Geochemical signatures of stratigraphic sequences and sea-
760 level change in the Woodford Shale, Permian Basin [M.Sc. thesis]: Golden ,
761 Colorado School of Mines, 89 p.

762

763 Mukhopadhyay, B., Brookins, D.G., and Bolivar, S.L., 1975, Rb-Sr whole-rock
764 study of the Precambrian rocks of the Pedernal Hills, New Mexico: Earth and
765 Planetary Science Letters, v. 27, p. 283-286.

766

767 Noble, P., 1992, Biostratigraphy of the Caballos Novaculite – Tesnus Formation
768 boundary, Marathon Basin, Texas: Palaeogeography, Palaeoclimatology,
769 Palaeoecology, v. 96, p. 141-153.

770

771 Perkins, R.B., Piper, D.Z., and Mason, C.E., 2008, Trace-element budgets in the
772 Ohio/Sunbury shales of Kentucky: Constraints on ocean circulation and primary
773 productivity in the Devonian-Mississippian Appalachian Basin:

774 Palaeogeography, Palaeoclimatology, Palaeoecology, v. 265, p. 14-29.

775

776 Schieber, J., 2003, Simple gifts and buried treasures – Implications of finding
777 bioturbation and erosion surfaces in black shales: The Sedimentary Record, v.
778 1, p. 4-8.

779

780 Schieber, J., and Riciputi, L., 2004, Pyrite ooids in Devonian black shales record
781 intermittent sea-level drop and shallow-water conditions: Geology, v. 32, p. 305–
782 308.

783

784 Schieber, J., and Southard, J.B., 2009, Bedload transport of mud by floccules
785 ripples – Direct observation of ripple migration processes and their implications:
786 *Geology*, v. 37, p. 483-486.

787

788 Schieber, J., and Yawar, Z., 2009, A new twist on mud deposition – Mud ripples
789 in experiment and rock record: *The Sedimentary Record*, v. 7, p. 4-8.

790

791 Schlager, W., Reijmer, J.J.G., and Droxler, A., 1994, Highstand shedding of
792 carbonate platforms: *Journal of Sedimentary Research*, v. B64, p. 270-281.

793

794 Sedlock, R.L., and Isozaki, Y., 1990, Lithology and biostratigraphy of Franciscan-
795 like cherts and associated rocks in west-central Baja California, Mexico:
796 *Geological Society of America*, v. 102, p. 852-864.

797

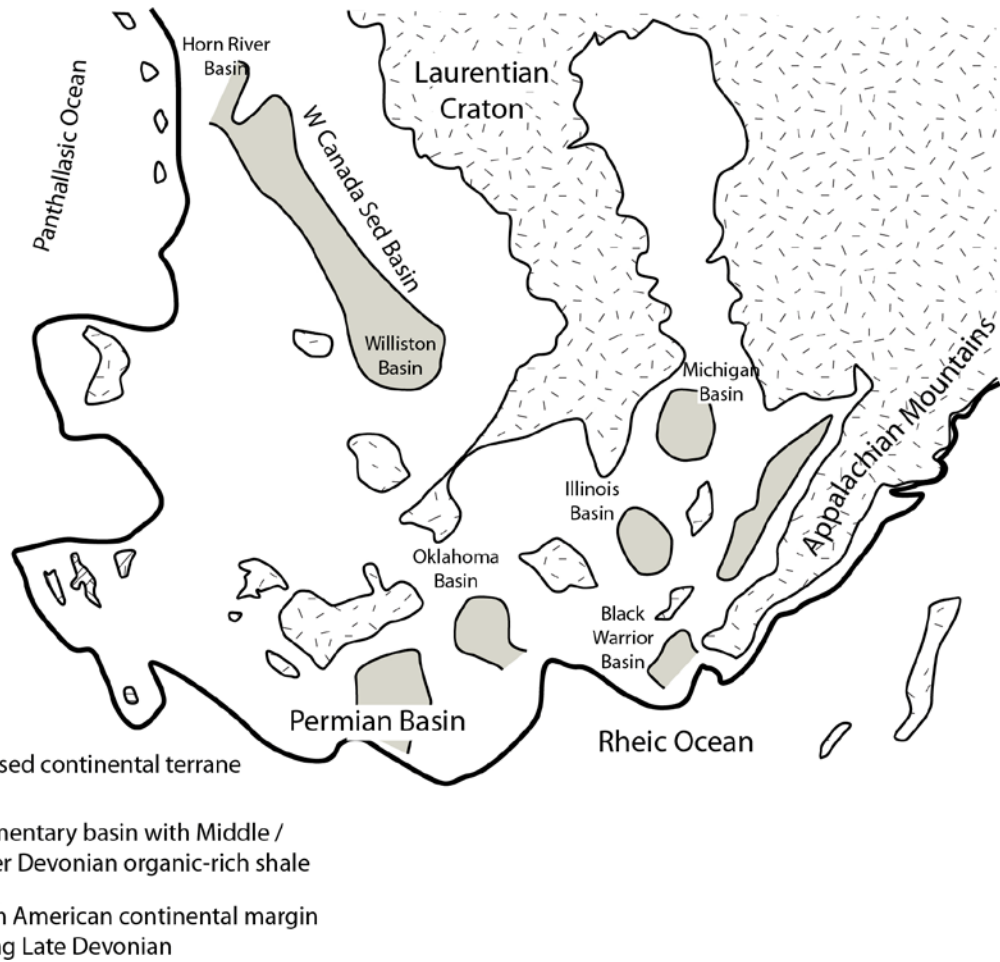
798 Swarbrick, E.E., 1967, Turbidite cherts from northeast Devon: *Sedimentary*
799 *Geology*, v. 1, p. 145-157.

800

801 Taylor, A.M., and Goldring, R., 1993, Description and analysis of bioturbation and
802 ichnofabric: *Journal of the Geological Society, London*, v. 150, p. 141-148.

803

804
805
806
807
808
809
810
811
812
813
814
815
816
817



818 Figure 1. Map of the North American continent in Late Devonian. Modified after
819 Algeo et al. (2007).

820

821

822

823

824

825

826

827

828

829

830

831

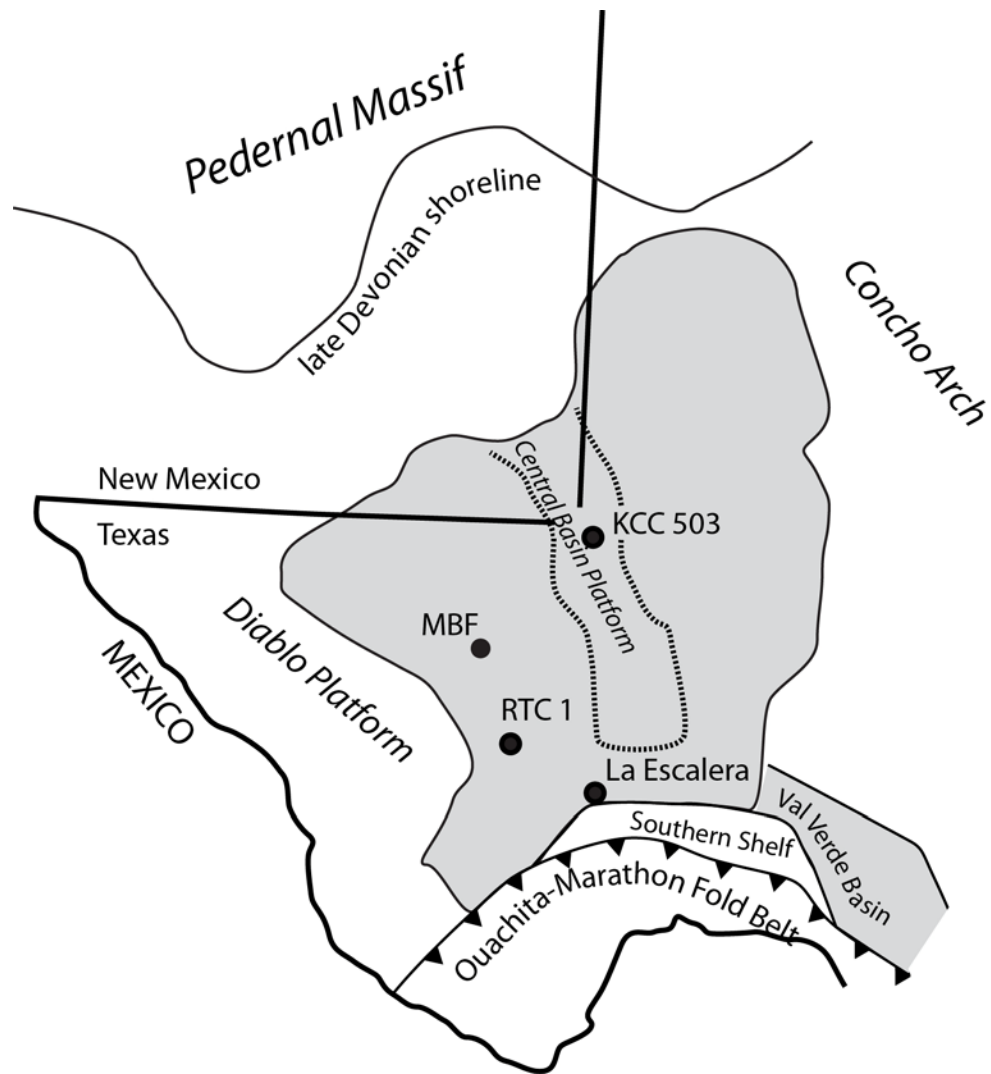
832

833

834

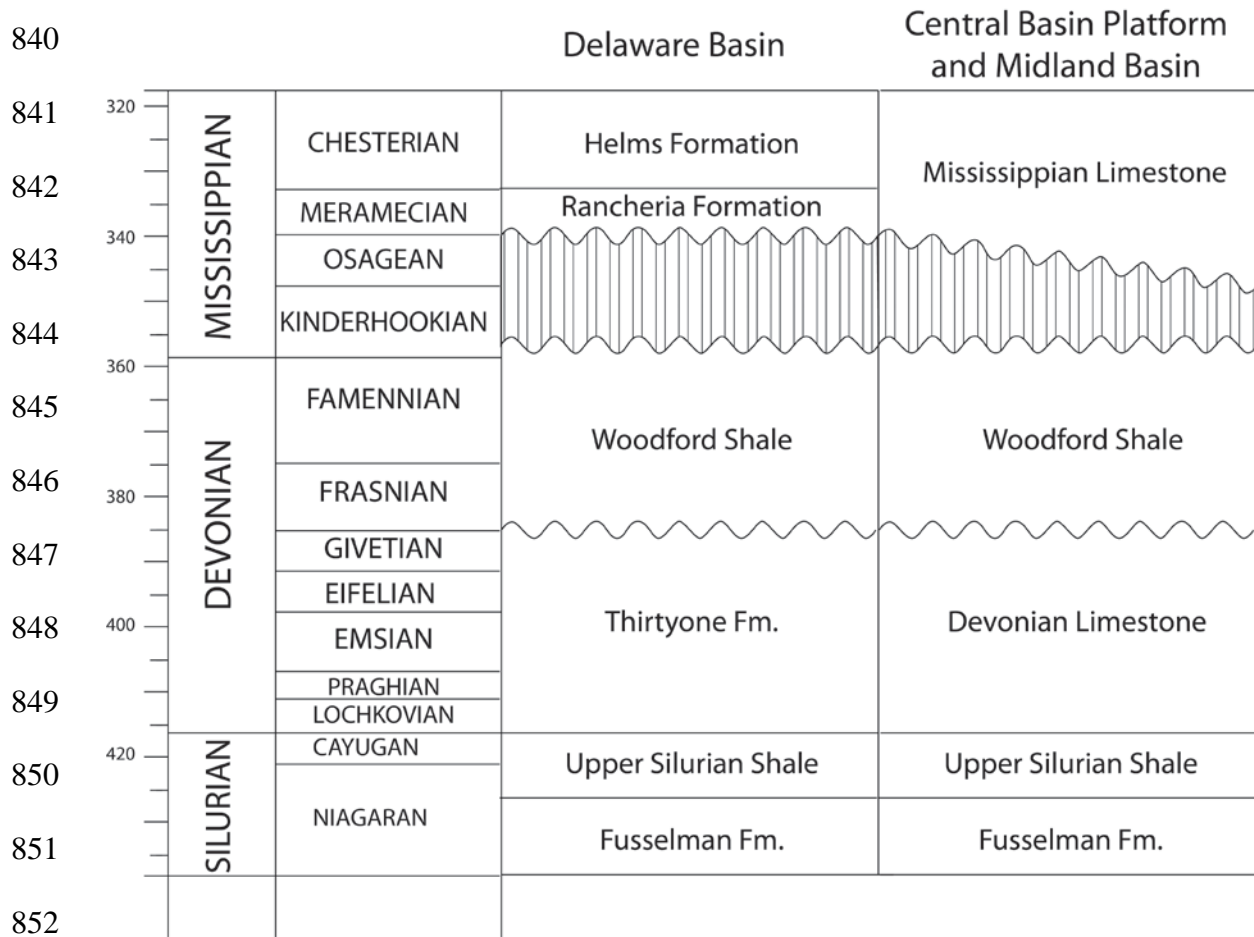
835

836



837 Figure 2. Map of the Permian Basin, showing locations of well included in the
838 study and key paleogeographic features.

839



852

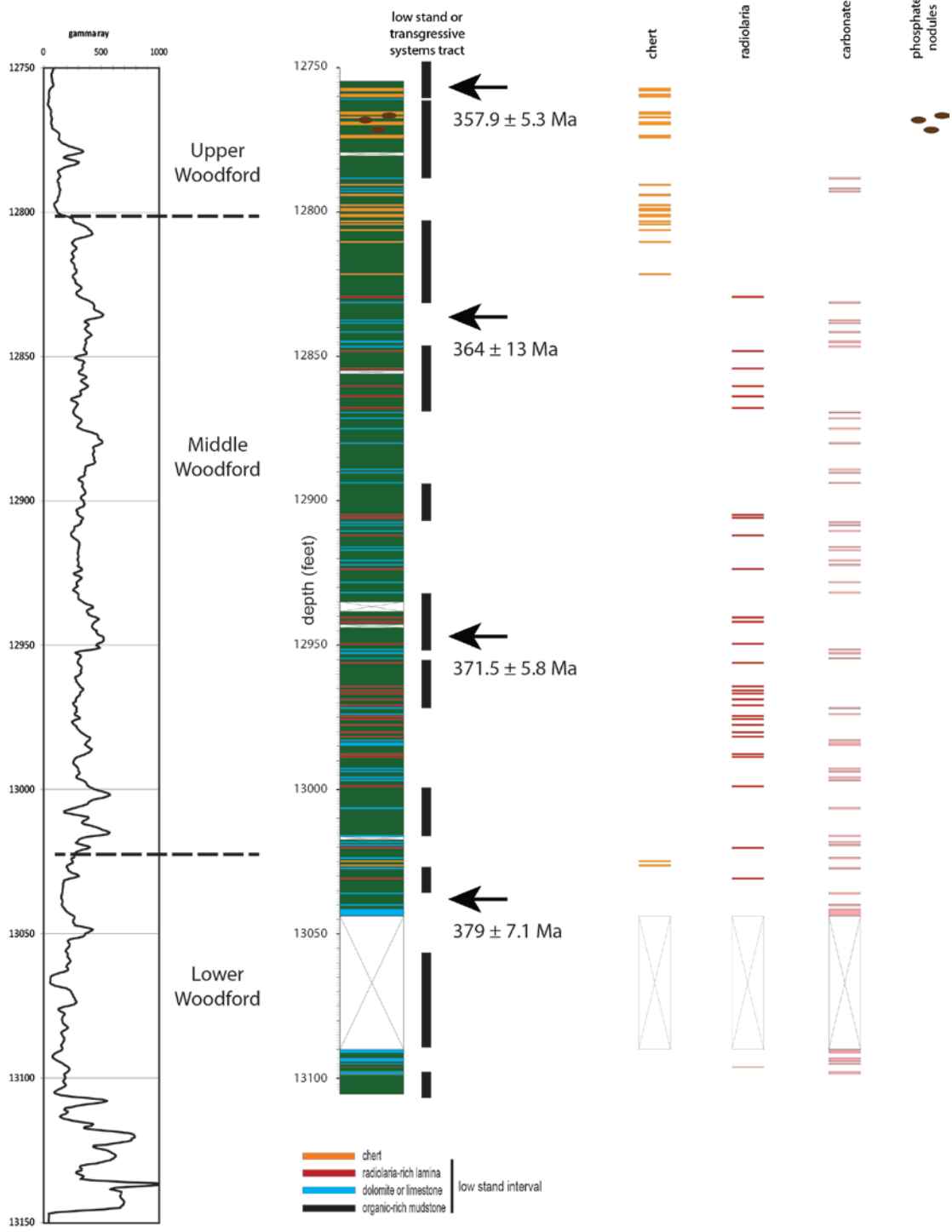
853

854 Figure 3. Silurian through Mississippian stratigraphy of the Permian Basin.

855 Modified after Comer (1991) and

856

857
 858
 859
 860
 861
 862
 863
 864
 865
 866
 867
 868
 869
 870
 871
 872
 873
 874
 875
 876
 877
 878
 879
 880
 881
 882
 883
 884
 885
 886
 887
 888
 889
 890
 891
 892
 893
 894
 895
 896
 897



898 Figure 4. Description of the RTC #1 core, Pecos County. Occurrences of non-
 899 mudstone facies (chert, radiolarian-rich laminae, carbonate beds, phosphate
 900 nodules) are highlighted in the four righthand columns, with thicknesses
 901 exaggerated for visibility. Black bars indicate intervals without carbonate beds,
 902 interpreted as low stand / transgressive intervals.

903
 904
 905
 906
 907
 908
 909
 910
 911
 912
 913
 914
 915
 916
 917
 918
 919
 920
 921
 922
 923
 924
 925
 926
 927
 928
 929
 930
 931
 932
 933
 934
 935
 936
 937
 938
 939
 940
 941
 942
 943
 944
 945
 946
 947
 948

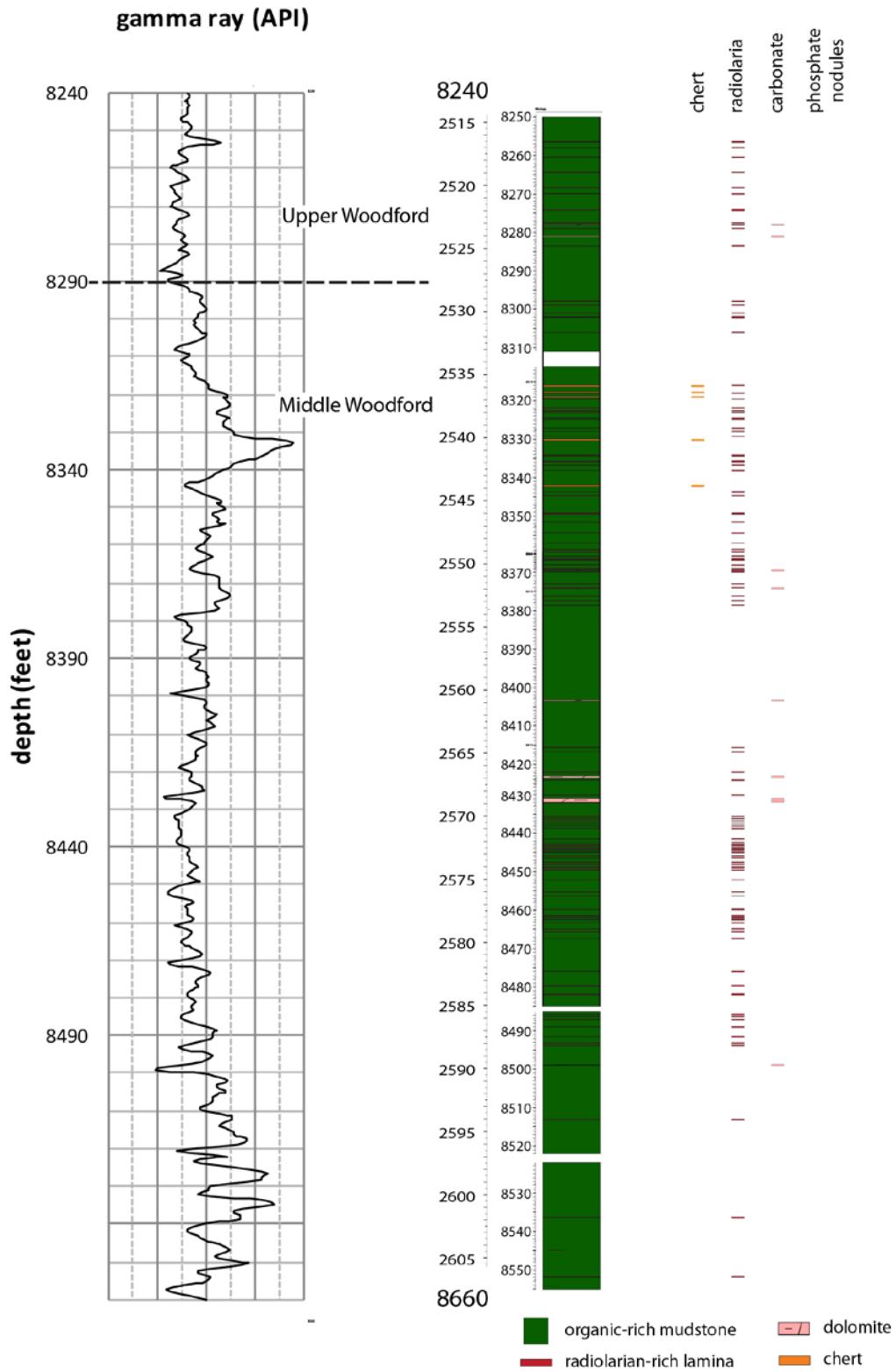


Figure 5. Description of the KCC 503 core, Winkler County. Symbols as in Figure 4.

949
 950
 951
 952
 953
 954
 955
 956
 957
 958
 959
 960
 961
 962
 963
 964
 965
 966
 967
 968
 969
 970
 971
 972
 973
 974
 975
 976
 977
 978
 979
 980
 981
 982
 983
 984
 985
 986
 987
 988
 989
 990
 991
 992
 993
 994

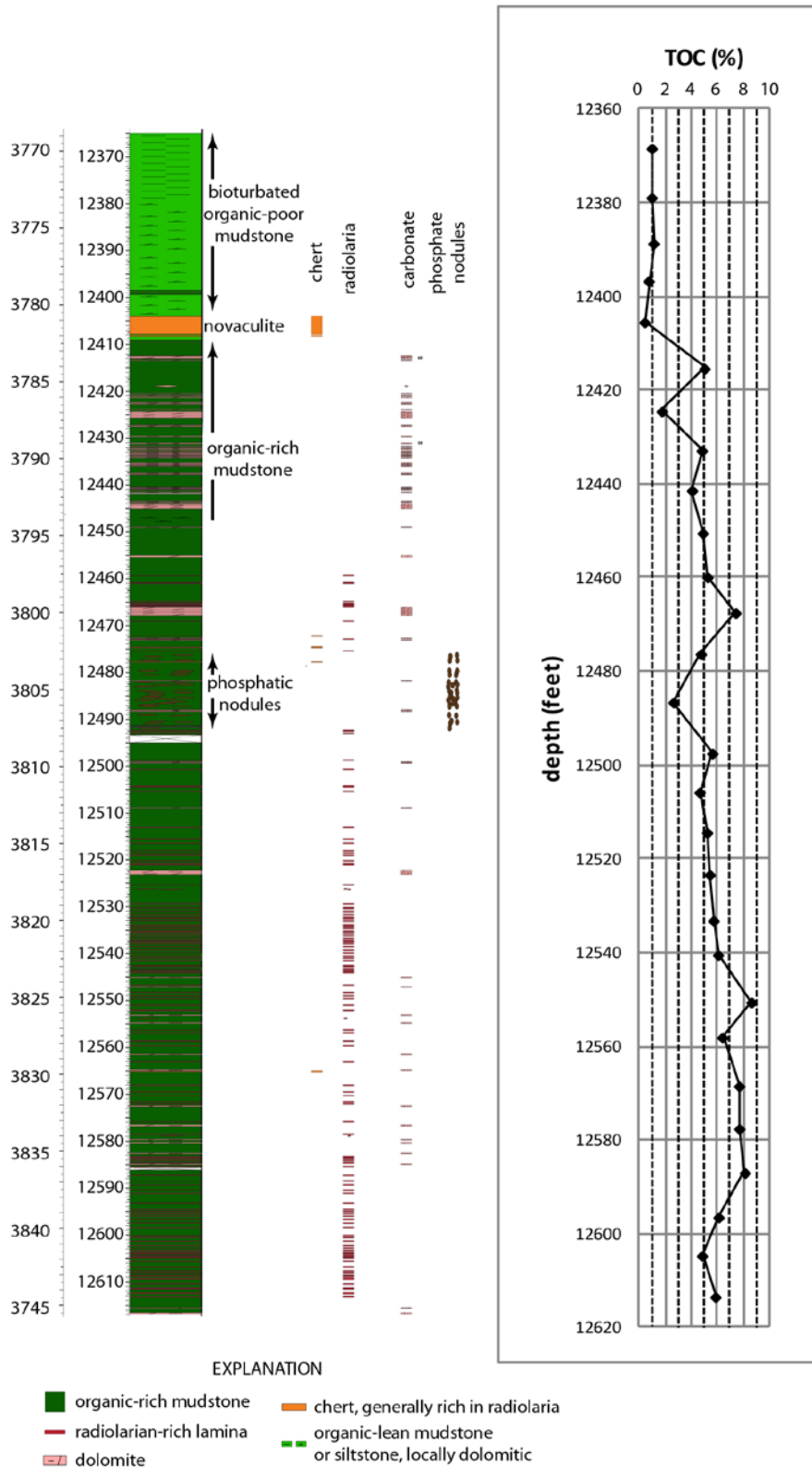


Figure 6. Description of the MBF core, Reeves Co. Symbols and description as in Figure 4.

995
 996
 997
 998
 999
 1000
 1001
 1002
 1003
 1004
 1005
 1006
 1007
 1008
 1009
 1010
 1011
 1012
 1013
 1014
 1015
 1016
 1017
 1018
 1019
 1020
 1021
 1022
 1023
 1024
 1025
 1026
 1027
 1028
 1029
 1030
 1031
 1032
 1033
 1034
 1035
 1036
 1037
 1038
 1039
 1040

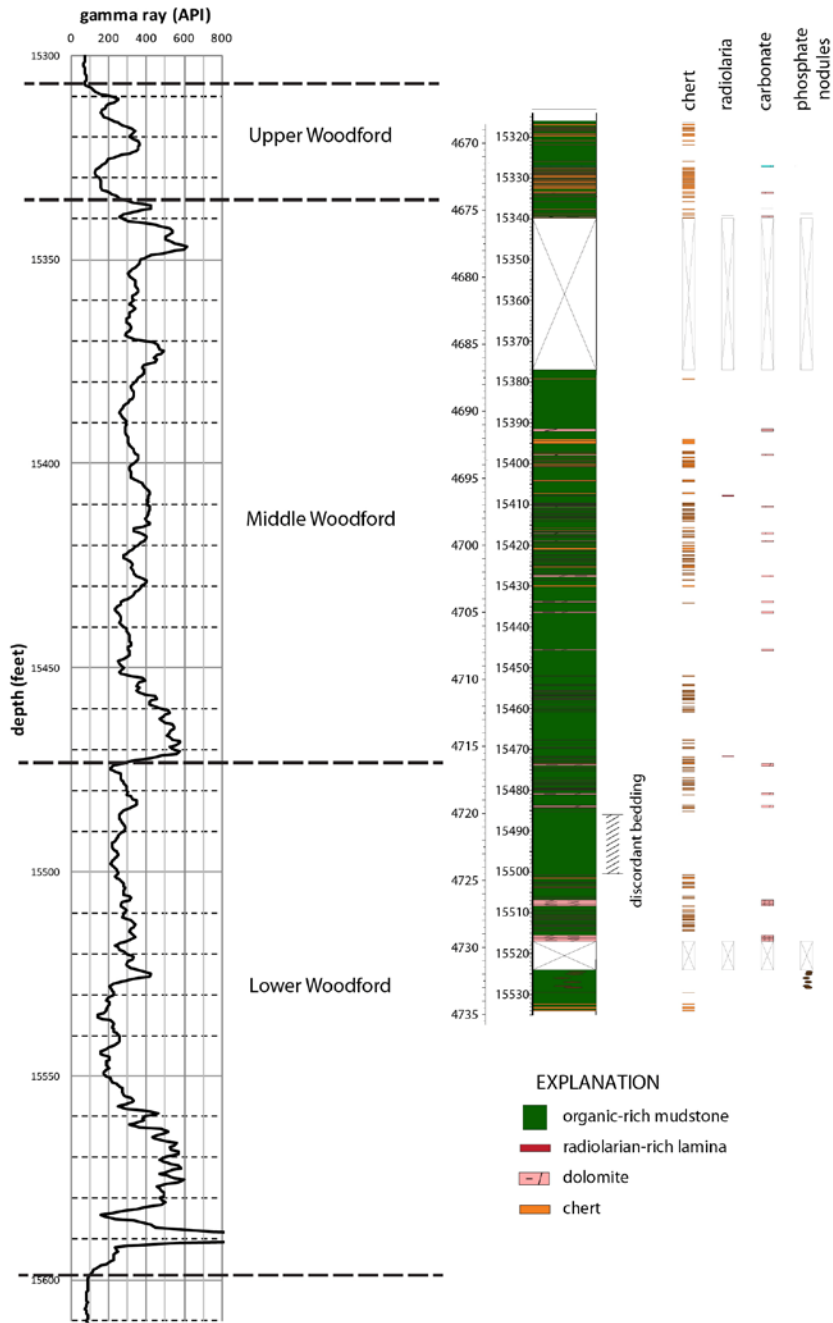


Figure 7. Description of the La Escalera B55 core, Winkler Co. Symbols and description as in Figure 4.

1041
1042
1043
1044
1045
1046
1047
1048
1049
1050
1051
1052
1053
1054
1055
1056
1057
1058
1059
1060
1061
1062
1063
1064
1065
1066
1067
1068
1069
1070
1071
1072
1073
1074
1075
1076
1077
1078
1079
1080
1081
1082
1083
1084
1085
1086

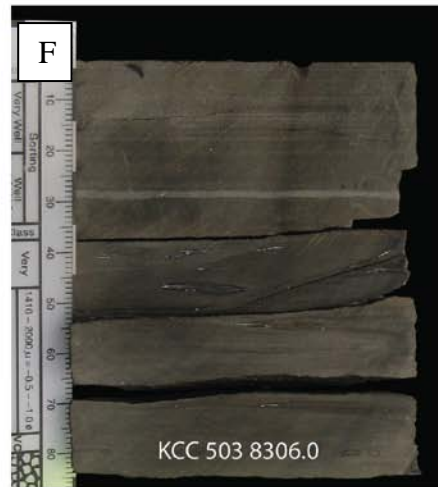


Figure 8.. Core photographs. A. Well-laminated mudstone. B. Massive or poorly laminated mudstone. C. Possible fluid escape structure. D. Syneresis cracks. E. Phosphate nodules in organic-rich mudstone. F. Radiolarian-rich lamina in laminated mudstone.

1087
1088
1089
1090
1091
1092
1093
1094
1095
1096
1097
1098
1099
1100
1101
1102
1103
1104
1105
1106
1107
1108
1109
1110
1111
1112
1113
1114
1115
1116
1117
1118
1119
1120
1121
1122
1123
1124

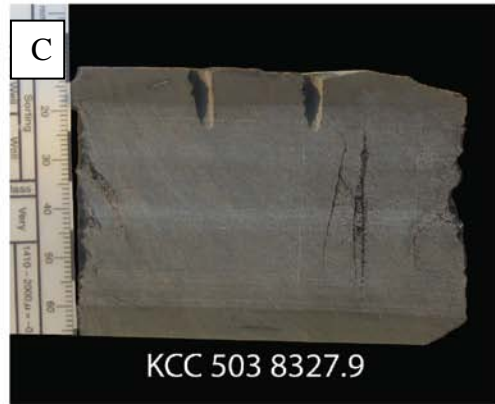


Figure 9. Core photographs. A. Dolomite bed. B. Dolomite bed with mudstone rip-up clasts. C. Chert bed. D. White and black novaculite. E. Bioturbated mudstone with large *Teichichnus* burrow.

1125
1126
1127
1128
1129
1130
1131
1132
1133
1134
1135
1136
1137
1138
1139
1140
1141
1142
1143
1144
1145
1146
1147
1148
1149
1150
1151
1152
1153
1154
1155
1156
1157
1158
1159
1160
1161
1162
1163
1164
1165
1166
1167
1168
1169
1170
1171

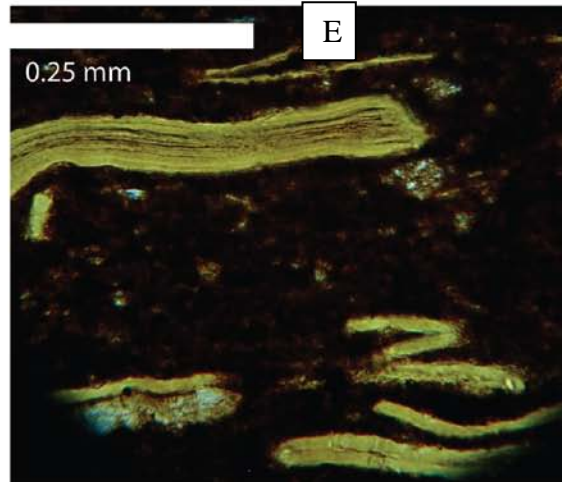
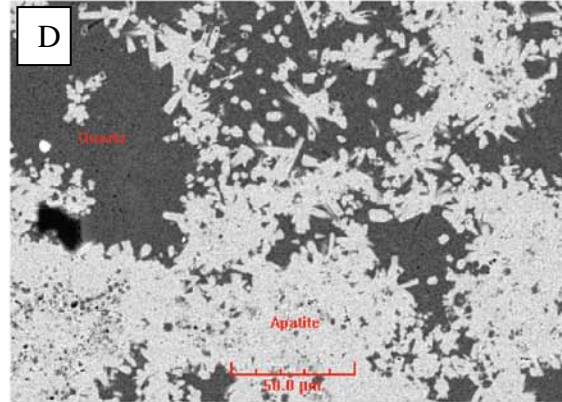
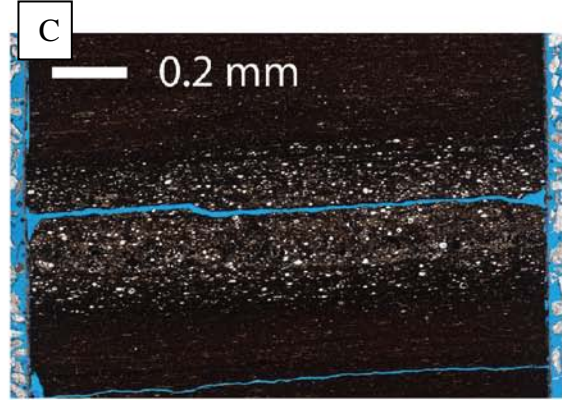
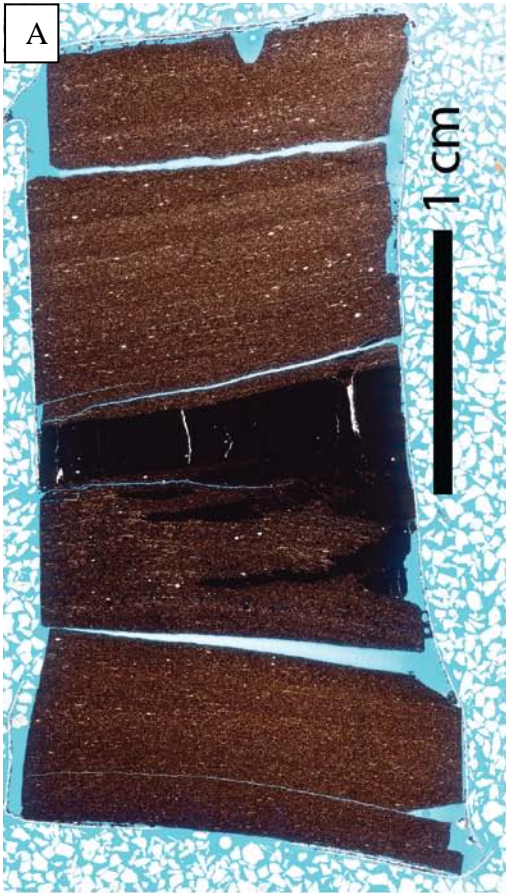


Figure 10. Thin section photographs. A. Laminated organic-rich mudstone. B. Dolomite bed. C. Radiolarian-rich lamina. D. Phosphate nodule. E. Tasmanites cysts in an organic-rich mudstone.

1172
1173
1174
1175
1176
1177
1178
1179
1180
1181
1182
1183
1184
1185
1186
1187
1188
1189
1190
1191
1192
1193
1194
1195
1196
1197
1198
1199
1200
1201
1202
1203
1204
1205
1206
1207
1208
1209
1210
1211
1212
1213
1214
1215
1216
1217

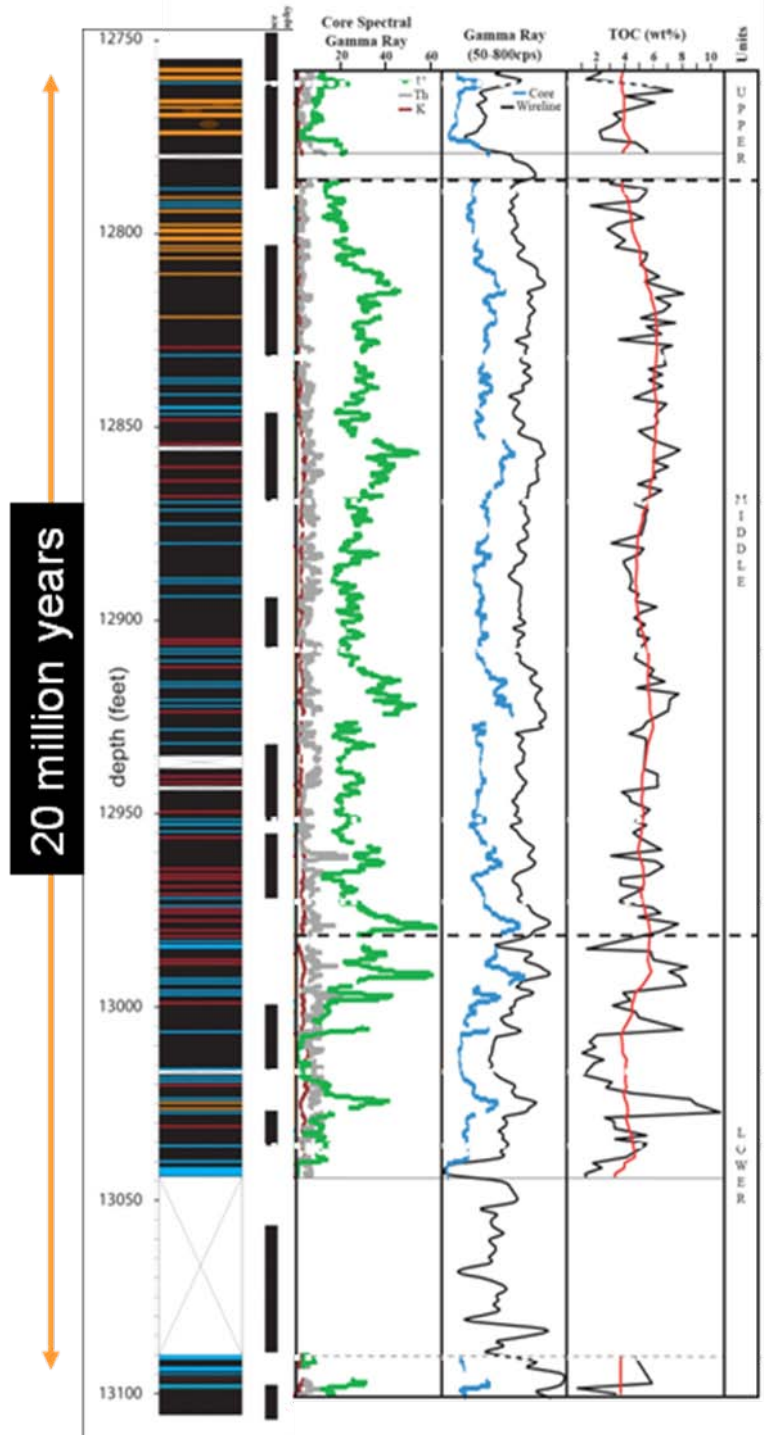


Figure 11. Description of the RTC#1 core, with core gamma (left track), total core gamma and wireline gamm (center track) and TOC (right track). The black bars represent interpreted low stand and transgressive systems tracts. In the core gamma data, brown represents potassium, grey thorium and green uranium. The red line in the TOC track represents a moving average over a 9 meter (30 feet) sliding window.